conf-890437--12

PNL-SA-16474

DE89 011214

PNL-SA--16474

MODELING GRAIN BOUNDARY MICRO-CHEMISTRY RELATED TO IASCC

E. P. Simonen
R. H. Jones

April 1989

Presented at the
CORROSION 89
New Orleans, Louisiana
April 20, 1989

Work supported by
the U.S. Department of Energy
under Contract DE-AC06-76RLO 1830

Pacific Northwest Laboratory
Richland, Washington 99352

DISCLAIMER

MODELING GRAIN BOUNDARY MICROCHEMISTRY RELATED TO IASCC

E. P. Simonen and R. H. Jones
Pacific Northwest Laboratory
Richland, WA 99352

ABSTRACT

Radiation effects on grain boundary and near grain boundary microchemistries are modeled and compared to measured radiation effects. Nonequilibrium diffusion mechanisms are shown to be consistent with measured phosphorus impurity segregation and measured chromium depletion resulting from irradiation. Radiation enhanced equilibrium segregation (impurity enrichment) and radiation enhanced chromium depletion (sensitization) kinetics are predicted to be sufficient to promote equilibrium effects but measurements do not confirm the radiation enhanced mechanisms. Likely causes for the discrepancy are solute trapping and precipitation effects in the matrix promoted by irradiation. Ion and neutron irradiation of austenitic steels are evaluated relative to causes for irradiation-assisted stress corrosion cracking (IASCC).

INTRODUCTION

Irradiation-Assisted Stress Corrosion Cracking (IASCC) is observed in austenitic stainless steels and nickel-base alloys exposed to light-water reactor environments and to neutron exposures greater than about 5×10^{20} neutrons/cm^2 ($E > 0.1$ MeV) or an equivalent of 1 displacement per atom (dpa).[1-5] Because the fracture mode for IASCC is intergranular, effects of radiation on grain boundary microchemistry have been suggested as causes for IASCC. Enrichment of impurities at boundaries and depletion of chromium are

considered to be the two most likely detrimental effects of irradiation on grain boundary microchemistry.

The mechanisms for impurity enrichment and for chromium depletion during irradiation are distinctly different from enrichment and depletion mechanisms during thermal annealing. Therefore, it is necessary to understand how environmental and material characteristics might affect IASCC compared to SCC without irradiation. The purpose of this paper is to describe models for radiation affected solute concentration near grain boundaries, to describe predicted environmental and material dependencies for these effects and to relate predictions to measured responses in austenitic stainless steels.

Radiation induced segregation mechanisms are nonequilibrium mechanisms distinctly different from thermally induced equilibrium mechanisms. Defect fluxes, induced by irradiation, couple with solute elements causing local solute enrichment or depletion near grain boundaries. The solute transport is supported dynamically by the irradiation flux and is not driven by thermodynamic activity gradients as is the case for thermal segregation. Consequently, segregation effects during irradiation will not be the same as known effects during thermal annealing with regard to elemental and environmental sensitivities.

During irradiation the degree of specific impurity enrichment is dictated by the binding energy between point defects and solute atoms.[6] During thermal annealing the degree of specific impurity segregation is dictated by the equilibrium isotherm.[7,8] The binding energy is an atomic size effect, whereas the equilibrium isotherm is a chemical effect. These distinct differences in the causes for segregation suggest that experience and intuition developed from thermal annealing studies of segregation are not related to expected effects from irradiation studies.

The kinetics of chromium depletion during irradiation are dictated by the difference in diffusion kinetics between chromium and other major alloying elements, namely, nickel.[9,10] Carbide precipitation on grain boundaries is not required for the radiation effect on chromium depletion as it is for the thermal effect.[11] The flux of irradiation produced vacancies to grain boundaries necessarily results in a flux of solute atoms away from the boundary. The slow diffusivity of nickel compared to chromium results in local enrichment of nickel and a local depletion of chromium near boundaries. This effect is known as the inverse Kirkendall effect because the defect flux causes a composition gradient in contrast to the conventional Kirkendall effect where a flux of atoms causes a defect gradient.

The kinetics of chromium depletion during thermal annealing is dictated by the diffusional growth of chromium carbides on grain boundaries.[11] The driving force for chromium depletion is a result of chromium concentration gradients in the matrix established by equilibrium of chromium in the matrix with chromium in the carbides. Depletion kinetics are controlled by the chromium diffusivity and are independent of the nickel diffusivity.

A further consideration when comparing irradiation versus thermal segregation is that irradiation can modify the matrix microstructure and

microchemistry such that elemental segregation may not be possible during irradiation. Impurities can be immobilized in traps or precipitates induced by the radiation. Particular examples include the formation of phosphides[12,13] and carbides.[14] Therefore, the availability of segregating elements during irradiation compared to thermal annealing also needs to be considered when assessing grain boundary microchemical causes for IASCC.

EXPERIMENTAL EVIDENCE FOR RADIATION INDUCED SEGREGATION

Evidence for redistribution of solute caused by irradiation have been established using Analytical Electron Microscopy (AEM) characterization of near grain boundary compositions[15-18], Auger analysis of fractured grain boundaries[19-21] and Auger sputter depth profiling of ion irradiated surfaces.[23-30] Most segregation measurements in irradiated materials have been made on relatively pure research alloys using ion irradiation of alloy surfaces in contrast to relatively impure commercial alloys using neutron irradiation of grain boundaries. The data strongly support the fundamental assumptions of the segregation theories but do not provide quantitative descriptions of grain boundary solute concentrations expected during IASCC.

Evidence for Radiation Induced Impurity Segregation

Ion irradiation experiments of nickel have clearly established that irradiation caused silicon segregation to the surfaces.[25-27,29,30] Radiation-induced segregation theories demonstrated that the segregation was nonequilibrium and was driven by diffusion of interstitial-solute complexes to free surfaces.[6] Similarly, segregation of silicon to grain boundaries was demonstrated. Additional experiments have since confirmed the theoretical prediction that undersized solutes (high interstitial binding) become enriched at boundaries and oversized solutes (low interstitial binding) become depleted at boundaries.

Segregation of phosphorus to ion irradiated surfaces in 316SS, Ni-P and PE-16 has also been measured.[22-24,31] Furthermore, the phosphorus segregation mechanism has been shown to be similar to that of silicon in nickel. Measured effects of manganese on radiation induced segregation of phosphorus implanted in an austenitic Fe-Ni-Cr alloy confirmed that the phosphorus mechanism was an interstitial diffusion mechanism and not a vacancy diffusion mechanism.[32]

Segregation of impurities to grain boundaries in neutron and electron irradiated stainless steels has also been observed. Phosphorus segregation to grain boundaries in 304 SS was measured using Auger spectroscopy after neutron irradiation.[21] However, the alloy was fractured at an elevated temperature, i.e., 550°C, and hence it was not clear if thermal segregation had occurred during the fracture test. Subsequently, phosphorus has been measured on exposed grain boundary surfaces in neutron irradiated 304 SS fractured at low temperature.[20] Although the measured phosphorus concentrations showed statistical variability, the phosphorus concentrations on intergranular surfaces were about five to twenty times greater than on transgranular fractured surfaces.

Segregation of impurities to grain boundaries in electron irradiated stainless steels has been measured using high voltage electron microscopy irradiations followed by analytical electron microchemical measurements of near grain boundary compositions.[15-17] These experiments have clearly indicated segregation of silicon to grain boundaries and some segregation of phosphorus to grain boundaries. The microchemical probe size was large compared to the spatial variations in composition and hence was limited in providing quantitative measurements near grain boundaries. None the less, these experimental results are consistent with observations of measured segregation of impurities to ion irradiated surfaces and neutron irradiated grain boundaries.

Evidence for Radiation Induced Alloy Segregation

Segregation of alloying elements during irradiation is evident in processes which occur during irradiation.[4,13,15-17,20,24,25,27,32-33] In particular, nickel silicides precipitate near defect sinks, such as voids and grain boundaries, in irradiated stainless steels.[33] The precipitation is caused by enrichment of nickel and silicon as a result of radiation-induced solute segregation. The silicon segregation effect was discussed in the previous section. A consequence of the nickel enrichment is the corresponding depletion in chromium and iron near grain boundaries.

The nickel enrichment and chromium depletion effect was initially interpreted in terms of the above interstitial segregation mechanism based on nickel being an undersized element and chromium being an oversized element.[26] Subsequently, a theory of segregation based on the inverse Kirkendall effect[9] was proposed to rationalize chromium depletion in neutron irradiated austenitic steel measured using analytical electron microchemical analysis. The chromium depletion width was about 20 nm for the neutron irradiation at 354°C and a dose rate of 1×10^{-8} dpa/s.[4] Similar chromium depletion widths were measured in electron irradiation steels and the depletion was found to depend on grain boundary migration during irradiation. Chromium depletion has also been measured using Auger sputter profiling of fractured irradiated grain boundaries. The depth of measured chromium depletion was only about 2 nm for the 304SS alloy irradiated at about 288°C at a dose rate of 9×10^{-7} dpa/s.[20]

MODELS FOR SEGREGATION DURING IRRADIATION

Three mechanisms for radiation affected segregation are presently considered: (1) nonequilibrium segregation for dilute solutions, (2) nonequilibrium segregation for concentrated solutions, and (3) radiation enhanced equilibrium segregation. Each of these three mechanisms is described below and predictions are given to demonstrated expected influences of material and irradiation parameters.

Radiation Induced Segregation - Dilute Solutions

The mechanism for radiation-induced segregation in dilute solutions has been modeled by Lam et al.[6] Solute trapping with mobile irradiation defects

results in redistribution of solutes near defect sinks. Significant effects are predicted for solutes which bind with self interstitials. Lesser effects are predicted for solute binding with vacancies.

Segregation is modeled by calculating the time and spatial dependence of radiation defects, solute and solute-defect complexes. The transport of solute-defect complexes to point defect sinks such as grain boundaries results in enrichment of solute near grain boundaries. The transport of solute occurs by uphill diffusion in opposition to an activity gradient. The contrast between equilibrium and nonequilibrium segregation mechanisms for dilute solutions is illustrated schematically in Figure 1.

For equilibrium segregation, the enrichment ratio between the boundary concentration and the equilibrium matrix concentration results in a concentration in the matrix at the boundary which is reduced compared to the bulk concentration. The reduced solute concentration causes downhill diffusion of solute to the boundary and a subsequent solute enrichment in the boundary until equilibrium is achieved and there is no concentration gradient.

For nonequilibrium segregation, the boundary concentration and the matrix concentration next to the boundary are assumed to be equal as shown in Figure 1. Solute transport to the boundary is driven by diffusion of solute-interstitial complexes to the boundary. Unbound solute can back diffuse into the matrix. A steady state profile will develop for which the back diffusion will balance the uphill diffusion.

The rate equations which describe the time and depth dependence of solute and defect species are shown in Equations 1 - 6 for each of the species considered.

$$\frac{dC_I}{dt} = \nabla(1 + \sigma_I C_s) D_I \nabla C_I + K_o - K_1 C_I C_V - K_2 C_I C_s + K_2' C_{Isa} - K_3 C_I C_s + K_3' C_{Isb} - K_5 C_I C_{Vs} \quad (1)$$

$$\frac{dC_V}{dt} = \nabla(1 + \sigma_V C_s) D_I \nabla C_I + K_o - K_1 C_I C_V - K_4 C_V C_s + K_4' C_{Vs} - K_6 C_V C_{Isa} - K_7 C_V C_{Isb} \quad (2)$$

$$\frac{dC_s}{dt} = \nabla(\sigma_I D_I C_s \nabla C_I - \sigma_V D_V C_s \nabla C_V) - K_2 C_I C_s + K_2' C_{Isa} - K_3 C_I C_s + K_3' C_{Isb} - K_4 C_V C_s + K_4' C_{Vs} + K_5 C_I C_{Vs} + K_6 C_V C_{Isa} + K_7 C_V C_{Isb} \quad (3)$$

$$\frac{dC}{dt}_{Isa} = D_{Isa} \nabla^2 C_{Isa} + K_2 C_I C_s - K_2' C_{Isa} - K_6 C_V C_{Isa} \quad (4)$$

$$\frac{dC}{dt}_{Isb} = K_3 C_I C_s - K_3' C_{Isb} - K_7 C_V C_{Isb} \quad (5)$$

$$\frac{dC}{dt}_{Vs} = D_{Vs} \nabla^2 C_{Vs} + K_4 C_V C_s - K_4' C_{Vs} - K_5 C_V C_{Vs} \qquad (6)$$

The six species include vacancies, C_v, interstitials, C_i, mobile solute-interstitial complexes, C_{Isa}, immobile solute-interstitial complexes, C_{Isb}, vacancy-solute complexes, C_{vs}, and untrapped solute, C_s. The GEAR integration routine is used to solve the one dimensional diffusion equations numerically. The 2 μm grain is divided into 22 regions ranging in width from 2.5 Angstroms at the grain boundary to 1,300 Angstroms at the center of the grain.[34] The diffusion coefficients are given by D and the capture factors for interstitials and vacancies are given by sigma. K_o is the defect production rate and K and K' are the rate constants for the reaction and dissolution of the species they modify.

Predicted dilute impurity segregation dependence on irradiation exposure, temperature and depth were calculated by Simonen and Jones[34] for conditions relevant to measured segregation of P to surfaces in stainless steel irradiated with ions. The calculated values compared to measure values are shown in Figure 2 for the ion irradiation dose rates and to a dose of one dpa.[31]

Using the best fit value of 0.6 eV for the binding energy for solute-interstitial traps, the predicted dose dependence and temperature dependence for neutron irradiation fluxes was made and is shown in Figure 3. The theory predicts that based on the measured strength of segregation using ions, the predicted segregation magnitude is expected to be near one monolayer for neutron irradiation conditions at grain boundaries.

The radiation theory does not require knowledge of the segregating species other than its binding energy with self interstitials. Therefore, the predictions could be equally applicable to segregation of elements other than phosphorus provided they bind strongly with self-interstitials.

Radiation Induced Segregation - Concentrated Solutions

Radiation induced segregation in concentrated solutions has been modeled by Perks et al.[10] based on the inverse Kirkendall effect. The change in local alloy composition occurs because of differences in elemental diffusivities. Nickel is a slow diffuser in stainless steel compared to chromium, therefore nickel becomes enriched near defect sinks and chromium becomes depleted near defect sinks (grain boundaries). The inverse Kirkendall mechanism is illustrated schematically in Figure 4.

Similar to the case of radiation-induced segregation in dilute solutions, the continuity equation is solved for iron, chromium and nickel as well as for vacancies and interstitials:[10]

$$\frac{dC}{dt}_j = -\frac{\nabla}{N} J_j \; . \qquad (7)$$

N is the atomic density; j is the atomic or defect species; and J is the flux. For atomic species, the flux equations for species, k, are given by

$$J_k = N [D_d \alpha \nabla C_k + C_k (d_{kv} \nabla C_v - d_{ki} \nabla C_i)]. \quad (8)$$

The thermodynamic factor, α, converts the concentration gradient to an activity gradient. The defect diffusivity is D_d. For vacancies and interstitials, the flux equations are given by

$$J_v = N [C_v \Sigma_k (d_{kv} \alpha \nabla C_k) - D_v \nabla C_v] \quad (9)$$

and

$$J_i = N [-C_i \Sigma_k (d_{ki} \alpha \nabla C_k) - D_i \nabla C_i]. \quad (10)$$

The partial atomic diffusivities are defined by d. Details of the equations and calculations can be found in Reference 10.

The calculations indicate that the width of chromium depleted zones could be of the order of 10 nm and chromium minimums at grain boundaries could be as low as 7%. Calculated chromium profiles[10] at 200 and 400°C are shown in Figure 5 and are compared to reported profiles[18,20] measured at one dpa. Qualitatively, the model predicts the measured profile for the AEM[18] results but predicts more chromium depletion than measured using sputter Auger profiling.[20]

The predicted temperature dependence of chromium concentration at the boundary is shown in Figure 6 for a neutron dose rate and at a dose of one dpa.[10] At high temperatures (above 600°C), the segregation vanishes because thermal vacancies outnumber irradiation produced vacancies and hence there is little flux of vacancies to grain boundaries. At low temperature (below 100°C), the segregation vanishes because mutual recombination of vacancies and interstitials prevents vacancy migration to grain boundaries. Most vacancies are annihilated by mutual recombination in the matrix at these low temperatures.

Radiation Enhanced Thermal Segregation

The driving forces for equilibrium impurity segregation and for chromium depletion exist for IASCC conditions as they do for thermal annealing conditions at higher temperatures. Without irradiation, the segregation mechanisms are not significant because the thermal diffusion kinetics are negligible at the low IASCC temperatures.[34] However, with irradiation there is the possibility that diffusion kinetics would be accelerated sufficiently to allow these high temperature mechanisms to occur at low temperatures.

Radiation Enhanced Equilibrium Segregation. The time dependence and equilibrium concentration for segregation of impurities can be calculated from the segregation theories of McLean[7] and Lea and Seah.[8] The surface concentration, CS, as a function of time, t, is given by

$$CS(t) = \alpha\, C_\infty\, [1 - \exp(D_S t/\alpha^2 d_w^2)\ \mathrm{erfc}(D_S t/\alpha^2 d_w^2)^{0.5}] \qquad (11)$$

D_S is the solute diffusivity, α is the enrichment ratio, d_w is the boundary thickness and C_∞ is the bulk solute concentration. The solute diffusivity during irradiation is calculated by multiplying the unirradiated diffusivity by the ratio of the vacancy concentration during irradiation, C_v, to the equilibrium vacancy concentration, C_{ve}. Therefore, the radiation enhanced diffusion coefficient, D^*, is

$$D^* = D_S C_v / C_{ve}. \qquad (12)$$

For phosphorus, D_S is assumed to be $0.51 \exp(-2.4/kT)$ cm^2/s.

For steady state irradiation and for an assumed rapid self interstitial migration, C_v is given by

$$C_v = (-b \pm \sqrt{(b^2 - 4*a*c)})/(2*a) \qquad (13)$$

$$a = 5.3 \times 10^{16}\ /s \qquad (14)$$

$$b = 10^9\ /cm^2 \qquad (15)$$

$$c = K_O/D_v. \qquad (16)$$

The vacancy diffusivity, D_v, is $0.0617 \exp(-1.28/kT)$ cm^2/s and the equilibrium vacancy concentration, C_{ve}, is assumed to be $\exp(-1.6/kT)$.

The surface concentration as a function of irradiation dose based on radiation enhanced phosphorus diffusion, i.e., Equation 12, was calculated for a dose rate of 5×10^{-3} dpa/s at 600°C as shown in Figure 7. The bulk solute concentration was assumed to be 5×10^{-4} atom fraction and the enrichment ratio was chosen to be 2000 to illustrate rates of achieving expected equilibrium concentrations accelerated by radiation enhanced diffusion. The measured phosphorus surface concentrations[24] as a function of dose are also shown in Figure 7. Radiation enhanced diffusion predictions exceed the measured surface concentrations.

For neutron conditions relevant to IASCC, the dose dependence of calculated grain boundary solute concentration is shown in Figure 8. The assumed temperature is 288°C and the assumed dose rate is 5×10^{-7} dpa/s. The effect of the assumed activation energy for solute diffusion is shown to illustrate expected effects for different solute elements. A value of 2.4 eV is reasonable for phosphorus diffusion, whereas a value of 2.7 eV is reasonable for silicon diffusion. The predictions indicate that radiation enhanced diffusion can result in significant levels of equilibrium solute enrichment for neutron irradiation conditions relevant to IASCC.

Radiation Enhanced Chromium Depletion. The effect of radiation on enhanced chromium depletion kinetics can be predicted from solutions to the one-dimensional diffusion equation. The depth dependence of chromium as a function of time is given by the following equation.[35]

$$C_{Cr}(x,t) = C_o + (C_\infty - C_o) \text{ erf } [x/(2\sqrt{(D^*_{Cr}t)}].$$

The radiation enhanced diffusivity, D_{Cr}^*, is calculated from the vacancy concentration indicated in Equation 13 times the vacancy diffusion coefficient.

The depth dependence of chromium concentration from a boundary is shown in Figures 9 and 10 for experiments reported by Jacobs et al.[20] and Norris et al.[18] The concentration profiles for three dpa levels are shown, i.e., 0.01, 0.1 and 1 dpa. In both cases, the calculated chromium depletion profiles at 1 dpa are much greater than the measured profiles. This indicates that radiation enhanced chromium diffusion can readily account for the measured chromium depletion profiles. Therefore, the lack of observed chromium carbides on the boundaries and the lack of observed chromium depletion is not caused by the lack of chromium diffusion kinetics at these neutron irradiation temperatures.

The calculated chromium depletion profiles for ion irradiation dose rates are shown in Figure 11 for 400, 500 and 600°C. The depth of the chromium depletion zone increases with increasing temperature and is expected to be of the order of 50 nm at 1 dpa if carbides are at grain boundaries in sufficient densities to ensure an equilibrium boundary concentration of the order of 8 atomic percent.

DISCUSSION

Models and experimental results for radiation effects on grain boundary microchemistries indicate that nonequilibrium segregation of impurities such as phosphorus and nonequilibrium depletion of chromium occur during radiation. The enrichment and depletion effects are similar to those which occur during thermal annealing without irradiation but occur by distinctly different mechanisms. Radiation is predicted to be necessary to promote significant kinetics for both the equilibrium and the nonequilibrium mechanisms. Thermal annealing kinetics are inadequate to allow significant effects without irradiation. The irradiation temperatures are low and times are short relative to temperatures and times at which equilibrium segregation and chromium depletion effects are observed for thermal annealing.

The above predictions have demonstrated that radiation can either induce nonequilibrium processes unique to radiation environments or it can accelerate the kinetics of equilibrium processes which occur in thermal environments.

Impurity Segregation

The model for nonequilibrium impurity segregation predicts that undersized solutes such as phosphorus and silicon will have strong binding with self interstitials and will segregate. Comparison of model predictions for phosphorus with measured surface concentrations induced by ion irradiation support the theoretical assumption of nonequilibrium segregation. Furthermore, the interstitial transport mechanism has been confirmed for phosphorus by Perks et al.[30] Measured depth profiles[24] near irradiated surfaces also indicates that the enrichment extends into the matrix and hence is not characteristic of monolayer segregation predicted by equilibrium theories. The phosphorus segregation behavior is similar to that of silicon in nickel which has been studied extensively and proven to be controlled by the nonequilibrium segregation mechanism.

The model for radiation enhanced equilibrium segregation predicts segregation kinetics much faster than measured kinetics. Predicted boundary concentrations shown in Figure 7 indicate that surface concentrations expected from radiation enhanced solute diffusion is about an order of magnitude faster than measured surface concentrations. The discrepancy between prediction and measurement suggests that mechanisms are operating which prevent radiation enhanced diffusion from occurring. A most likely mechanism is that the impurity is being trapped or precipitated and is immobilized in the matrix. There is evidence for example that irradiation can promote phosphide precipitates.[12,13] Alternatively, the discrepancy between predicted and measured surface concentrations shown in Figure 7 may be caused by loss mechanisms of phosphorus at the surface during irradiation. Loss mechanisms such as sputtering or evaporation may have occurred.

Chromium Depletion

The model for nonequilibrium chromium depletion predicts radiation-induced chromium depletion profiles similar to measured profiles for neutron irradiations at 354°C and at relatively low dose rates, 1×10^{-8} dpa/s.[22] Irradiation at 288°C and at 9×10^{-7} dpa/s resulted in profiles much narrower than predicted.[20] Therefore, qualitatively, the nonequilibrium model (inverse Kirkendall effect) is consistent with measured effects although the model has not been as extensively verified as for nonequilibrium impurity segregation.

Predictions of radiation enhanced chromium depletion caused by grain boundary carbide precipitation indicate that grain boundary carbide precipitation is expected at both ion and neutron irradiation conditions of interest. Experimentally, grain boundary carbide precipitation is not observed during irradiation.[31] Calculated chromium depletion profiles based on radiation enhanced diffusion of chromium are much wider than measured profiles indicating that carbides are not present at the boundaries at sufficient density to produce diffusion of chromium down an activity gradient toward the boundary. It is expected that grain boundary carbides would nucleate during irradiation based on the high radiation enhanced chromium diffusivity. A likely cause for the absence of carbides is that the carbon is precipitated in the matrix during irradiation and is not available for

grain boundary precipitation.[14] Also, chromium depletion at the boundary caused by the inverse Kirkendall effect may be rapid compared to the time required for carbide nucleation.

CONCLUSIONS

Nonequilibrium mechanisms rationalize measured radiation effects on impurity segregation to boundaries and chromium depletion near boundaries. Equilibrium mechanisms have insufficient kinetics to promote these microchemical changes without irradiation at the irradiation temperatures and times. Calculated radiation enhanced diffusion of impurities and chromium has been shown to result in adequate kinetics to promote equilibrium segregation of impurities and depletion of chromium which are not observed. It is proposed that precipitation of phosphides and carbides in the matrix could account for the lack of evidence for radiation enhanced equilibrium solute segregation and chromium depletion effects.

ACKNOWLEDGMENTS

This work supported by the Materials Sciences Branch, Office of Basic Energy Sciences, U.S. Department of Energy, under Contract DE-AC06-76RLO 1830.

REFERENCES

1. F. Garzarolli, D. Alter, P. Dewes, and J. L. Nelson, "Deformability of Austenitic Stainless Steels and Ni-Based Alloys in the Core of a Boiling and a Pressurized Water Reactor," Proceedings of the Third International Symposium on Environmental Degradation of Materials in Nuclear Power-Systems - Water Reactors, Eds., G. J. Theus and J. R. Weeks, The Metallurgical Society, Warendale, PA, 1988.

2. A. J. Jacobs, G. P. Wozadlo, K. Nakata, T. Yoshida, and I. Masaoka, "Radiation Effects on the Stress Corrosion and Other Selected Properties of Type-304 and Type-316 Stainless Steels," Proceedings of the Third International Symposium on Environmental Degradation of Materials in Nuclear Power-Systems - Water Reactors, Eds., G. J. Theus and J. R. Weeks, The Metallurgical Society, Warendale, PA, 1988.

3. A. J. Jacobs and G. P. Wozadlo, "Irradiation-assisted Stress Corrosion Cracking as a Factor in Nuclear Power Plant Aging," Proceedings of the International Conference on Nuclear Power Plant Aging Availability Factor and Reliability Analysis, Ed. V. S. Goel, American Society for Metals, Metals Park, OH, 1985.

4. D. I. R. Norris editor, Proceedings of Symposium on Radiation-induced Sensitization of Stainless Steels held at Berkeley Nuclear Laboratories, September 1986, CEGB, INIS-GB-90.

5. H. Hanninen and I. Aho-Mantilla, "Environment-Sensitive Cracking of Reactor Internals," p. 77, Proceedings of the Third International Symposium on Environmental Degradation of Materials in Nuclear Power-Systems - Water Reactors, Eds., G. J. Theus and J. R. Weeks, The Metallurgical Society, Warendale, PA, 1988.

6. N. Q. Lam, P. R. Okamoto, H. Wiedersich and A. Taylor, Metallurgical Transactions, 9A, p. 1707 (1978).

7. D. McLean, in Grain Boundaries in Metals, Oxford University Press, London, chapter 5, 1957.

8. C. Lea and M. P. Seah, Philosophical Magazine, Vol. 35, p. 213, (1977).

9. A. D. Marwick, J. Phys. F: Metal Phys., Vol. 8, p. 1849, (1978).

10. J. M. Perks, A. D. Marwick and C. A. English, "Fundamental Aspects of Radiation-Induced Segregation in Fe-Cr-Ni Alloys," p. 15, in Proceedings of Symposium on Radiation-induced Sensitization of Stainless Steels held at Berkeley Nuclear Laboratories, D. I. R. Norris editor, September 1986, CEGB, INIS-GB-90.

11. E. C. Bain and R. H. Aborn, Trans. Am. Soc. Steel Treat., Vol. 18, p. 837, (1930).

12. E. H. Lee and L. K. Mansur, Journal of Nuclear Materials, Vol. 141-143, p. 695, (1986)

13. Kiyotomo Nakata and Isao Masaoka, Journal of Nuclear Materials, Vol. 150, p. 196, (1987).

14. F. A. Garner and D. S. Gelles, "Irradiation Creep Mechanisms: An Experimental Perspective," in Proceedings of the International Workshop on Mechanisms of Irradiation Creep and Growth, held June 1987, to be published in Journal of Nuclear Materials.

15. K. Fukuya, S. Nakahigashi, and M. Terasawa,, Scripta Metallurgica, Vol. 19, p. 959, (1985).

16. Kiyotomo Nakata, Yoshio Katanom Isao Masaoka and Kensuke Shiraishi, Journal of Nuclear Materials, Vols. 133&134, p. 575, (1985).

17. K. Fukuya, S. Nakahigashi, M. Terasawa and S. Shima, "Grain Boundary Segregation of Impurity Atoms in Irradiated Austenitic Stainless Steels," Proceedings of the Third International Symposium on Environmental Degradation of Materials in Nuclear Power-Systems - Water Reactors, Eds., G. J. Theus and J. R. Weeks, The Metallurgical Society, Warendale, PA, 1988.

18. D. I. R. Norris, C. Baker and J. M. Titchmarsh, "Compositional Profiles at Grain Boundaries in 20%Cr/25%Ni/Nb Stainless Steel," p. 86, in Proceedings of Symposium on Radiation-induced Sensitization of Stainless Steels held at Berkeley Nuclear Laboratories, D. I. R. Norris editor, September 1986, CEGB, INIS-GB-90.

19. R. E. Clausing and E. E. Bloom, "Auger Electron Spectroscopy of Fracture Surfaces in Irradiated Type 304 Stainless Steel," p. 491, in Grain Boundaries in Engineering Materials, Claitors, Baton Rouge, LA, (1975).

20. A. J. Jacobs, R. E. Clausing, L. Heatherly and R. M. Kruger, "Irradiation-Assisted Stress Corrosion Cracking and Grain Boundary Segregation in Heat Treated Type-304 SS," in 14th International ASTM Symposium on the Effects of Radiation on Materials held in Andover, MA, June 1988, to be published.

21. K. Farrell, N. Kishimoto, R. E. Clausing, L. Heatherly and G. L. Lehman, Journal of Nuclear Materials, Vols. 141-143, p. 991, (1986).

22. J. L. Brimhall, D. R. Baer, and R. H. Jones, Journal of Nuclear Materials, Vols. 103 & 104, p. 1379, (1981).

23. J. L. Brimhall, D. R. Baer, and R. H. Jones, Journal of Nuclear Materials, Vol. 117, p. 218, (1983).

24. J. L. Brimhall, D. R. Baer, and R. H. Jones, Journal of Nuclear Materials, Vols. 122 & 123, p. 196, (1984).

25. V. K. Sethi and P. R. Okamoto, "Radiation-Induced Segregation in Complex Alloys," in proceedings on Phase Stability During Irradiation, Ed. J. R. Holland, L. K. Mansur and D. I. Potter, p. 109, AIME, New York, NY., (1981).

26. P. R. Okamoto and H. Wiedersich, Journal of Nuclear Materials, Vol. 53, p. 336, (1974).

27. L. E. Rehn, P. R. Okamoto, D. I. Potter and H. Wiedersich, Journal of Nuclear Materials, Vol. 74, p. 242, (1978).

28. R. A. Erck, D. I. Potter and H. Wiedersich, Journal of Nuclear Materials, Vol. 80, p. 120, (1979).

29. L. E. Rehn, P. R. Okamoto and H. Wiedersich, Journal of Nuclear Materials, Vol. 80, p. 172, (1979).

30. L. E. Rehn, P. R. Okamoto, D. I. Potter and H. Wiedersich, "Radiation-Induced Segregation in Nickel-Silicon Alloys," in Effects of Radiation on Structural Materials, ASTM STP 683, p. 184, Ed., J. A. Sprague and D. Kramer, American Society for Testing and Materials, Philadelphia, PA (1979).

31. E. P. Simonen, E. R. Bradley and R. H. Jones, "Segregation to Surfaces in Irradiated Stainless Steels," in 14th International ASTM Symposium on the Effects of Radiation on Materials held in Andover, MA, June 1988, to be published.

32. J. M. Perks, C. A. English and M. L. Jenkins, "Radiation-Induced Segregation of Phosphorus in Nickel and in Fe-Cr-Ni Alloys," in 14th International ASTM Symposium on the Effects of Radiation on Materials held in Andover, MA, June 1988, to be published.

33. W. J. S. Yang, H. R. Brager and F. A. Garner, "Radiation-Induced Phase Development in AISI 316," p. 257, in proceedings on Phase Stability During Irradiation, Ed. J. R. Holland, L. K. Mansur and D. I. Potter, AIME, New York, NY., (1981).

34. E. P. Simonen and R. H. Jones, "Calculated Solute Segregation Kinetics Related to Irradiation Assisted Stress Corrosion Cracking," p. 683, Proceedings of the Third International Symposium on Environmental Degradation of Materials in Nuclear Power-Systems - Water Reactors, Eds., G. J. Theus and J. R. Weeks, The Metallurgical Society, Warendale, PA, 1988.

35. P. G. Shewmon, Diffusion in Solids, McGraw-Hill, New York, N. Y., p. 14, 1963.

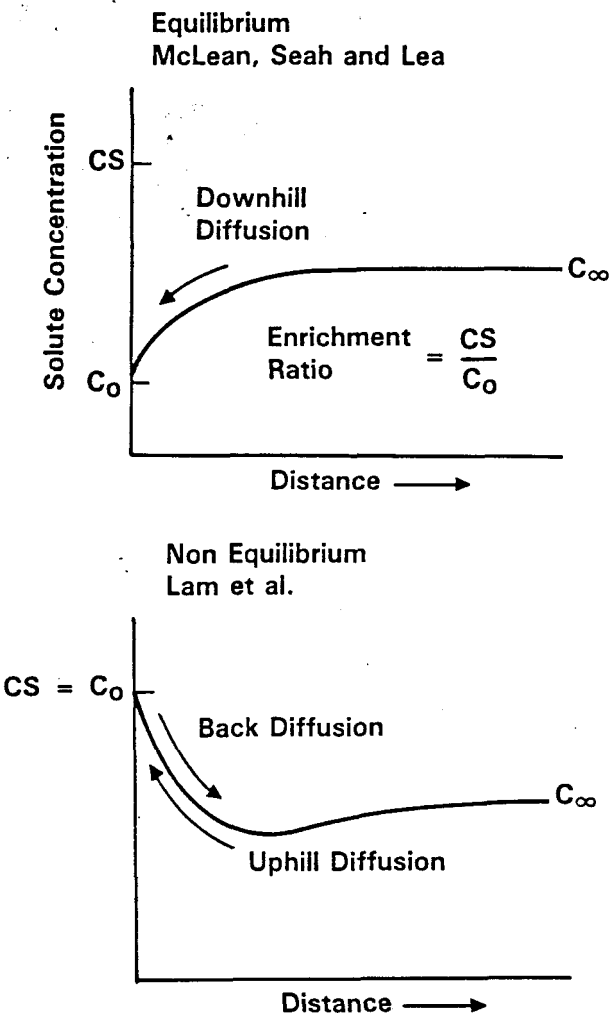

FIGURE 1 - Schematic of equilibrium and nonequilibrium solute segregation mechanisms.6-8

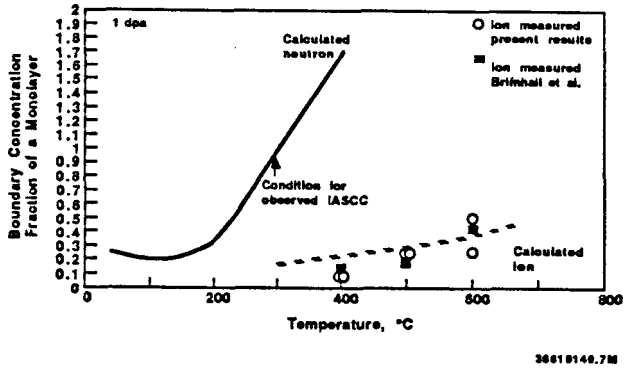

Figure 2 - Comparison of calculated and measured surface concentration of phosphorus after one dpa on ion irradiation.24,31

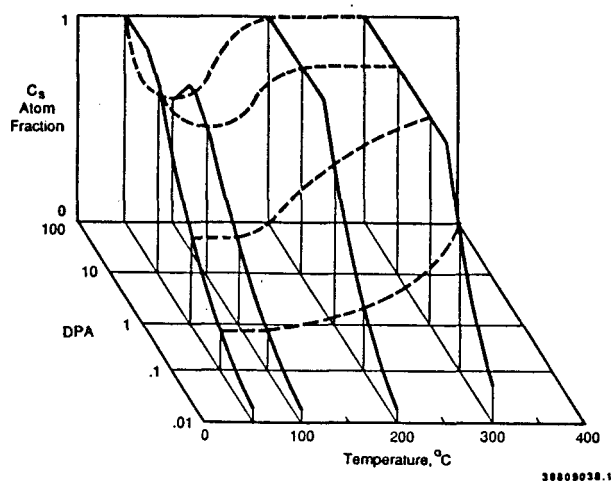

Figure 3 - Calculated dose and temperature dependence of boundary solute concentration based on theory calibrated in Figure 2.

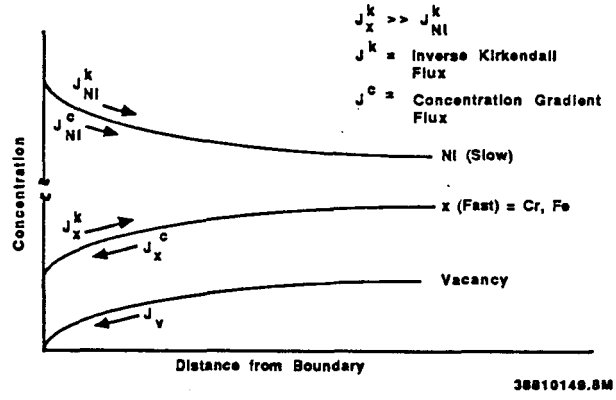

Figure 4 - Schematic of non-equilibrium chromium depletion according to the inverse Kirkendall mechanism.

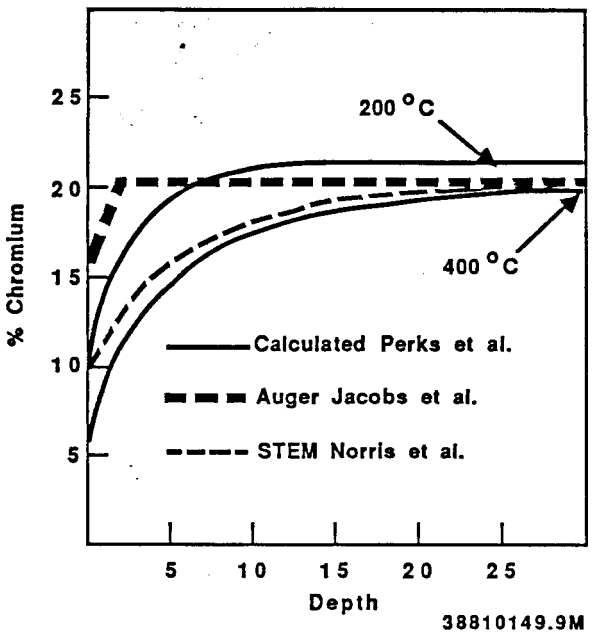

Figure 5 - Comparison of calculated nonequilibrium chromium depletion[10] compared to measured chromium depletion profiles.[18,20]

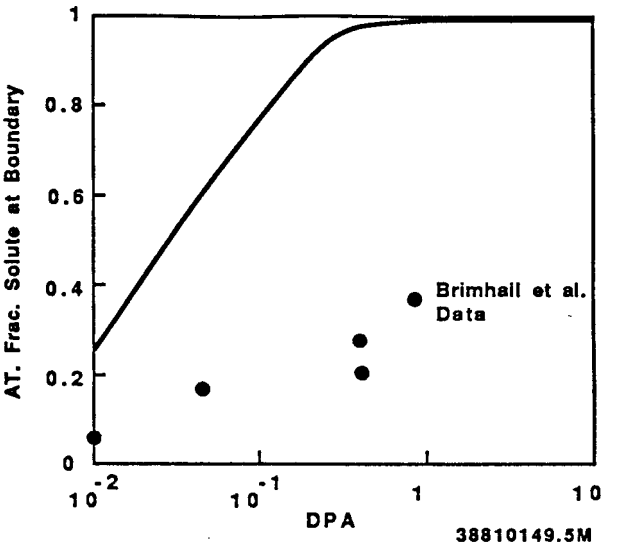

Figure 7 - Calculated phosphorus boundary concentration versus dpa based on radiation enhanced segregation compared to measurements of Brimhall et al.[24]

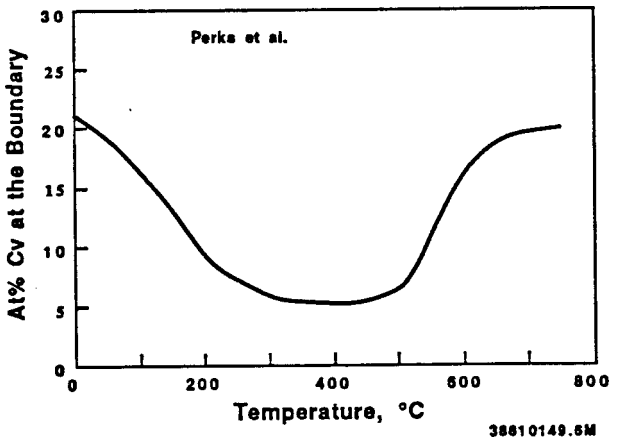

Figure 6 - Calculated temperature dependence of chromium boundary concentration from Perks et al.[10]

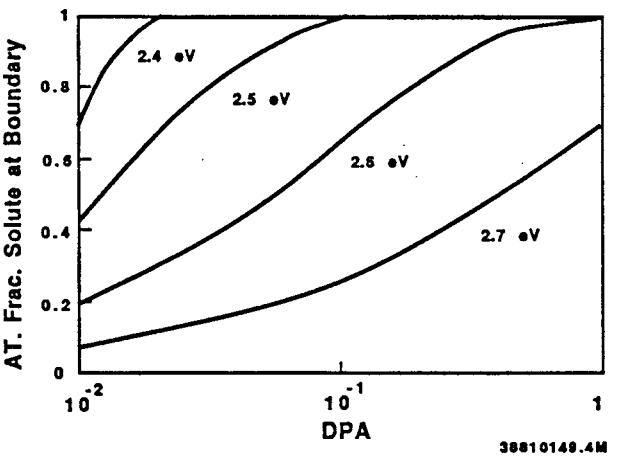

Figure 8 - Calculated impurity boundary concentration versus dpa based on assumed activation energy for impurity diffusion during neutron irradiation.

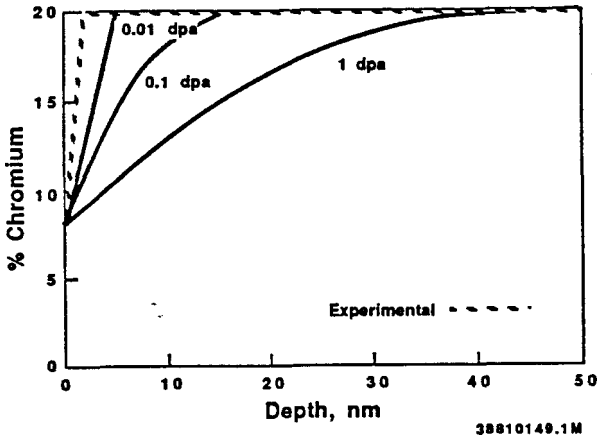

Figure 9 - Calculated radiation enhanced chromium depletion compared to measurements of Jacobs et al.[20]

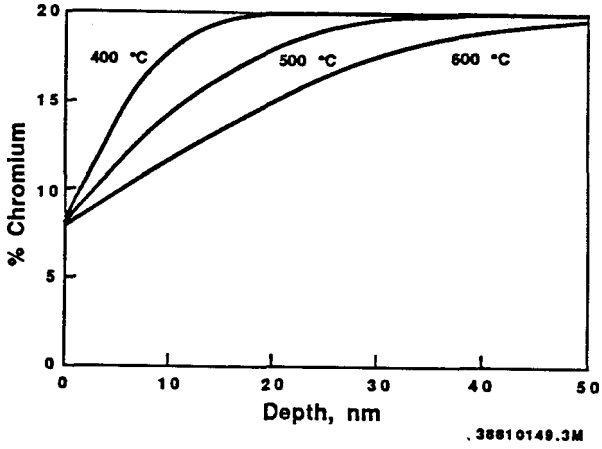

Figure 11 - Calculated radiation enhanced chromium depletion based on an ion irradiation dose rate of 5×10^{-3} dpa/s and 1 dpa.

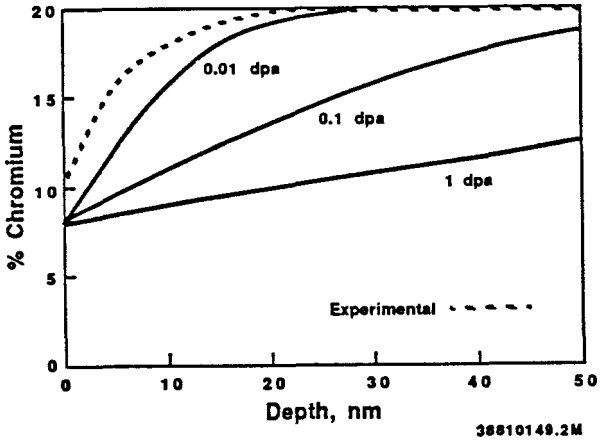

Figure 10 - Calculated radiation enhanced chromium depletion compared to measurements of Norris et al.[18]